



ALMA MATER STUDIORUM  
UNIVERSITÀ DI BOLOGNA

ARCHIVIO ISTITUZIONALE  
DELLA RICERCA

## Alma Mater Studiorum Università di Bologna Archivio istituzionale della ricerca

Investigating the influence of the grain size and distribution on the macroscopic dielectric properties of Antarctic firn

This is the final peer-reviewed author's accepted manuscript (postprint) of the following publication:

*Published Version:*

Olmi R., Bittelli M., Picard G., Arnaud L., Mialon A., Priori S. (2021). Investigating the influence of the grain size and distribution on the macroscopic dielectric properties of Antarctic firn. COLD REGIONS SCIENCE AND TECHNOLOGY, 185(May 2021), 1-10 [10.1016/j.coldregions.2021.103254].

*Availability:*

This version is available at: <https://hdl.handle.net/11585/813154> since: 2021-03-07

*Published:*

DOI: <http://doi.org/10.1016/j.coldregions.2021.103254>

*Terms of use:*

Some rights reserved. The terms and conditions for the reuse of this version of the manuscript are specified in the publishing policy. For all terms of use and more information see the publisher's website.

This item was downloaded from IRIS Università di Bologna (<https://cris.unibo.it/>).  
When citing, please refer to the published version.

(Article begins on next page)

This is the final peer-reviewed accepted manuscript of:

R. Olmi, M. Bittelli, G. Picard, L. Arnaud, A. Mialon, S. Priori,

*Investigating the influence of the grain size and distribution on the macroscopic dielectric properties of Antarctic firn,*

Cold Regions Science and Technology, Volume 185, 2021, 103254, ISSN 0165-232X,

The final published version is available online at:

<https://doi.org/10.1016/j.coldregions.2021.103254>.

Terms of use:

Some rights reserved. The terms and conditions for the reuse of this version of the manuscript are specified in the publishing policy. For all terms of use and more information see the publisher's website.

This item was downloaded from IRIS Università di Bologna (<https://cris.unibo.it/>)

When citing, please refer to the published version.

# Cold Regions Science and Technology

## Investigating the influence of the grain size and distribution on the macroscopic dielectric properties of Antarctic Firn

--Manuscript Draft--

<b>Manuscript Number:</b>	
<b>Article Type:</b>	Research Paper
<b>Keywords:</b>	Antarctica, dielectric measurements, ice cores, dielectric model, full wave EM simulations, firn
<b>Corresponding Author:</b>	MARCO BITTELLI University of Bologna Bologna, WA ITALY
<b>First Author:</b>	Roberto Olmi, PhD
<b>Order of Authors:</b>	Roberto Olmi, PhD MARCO BITTELLI Ghislain Picard, PhD Laurent Arnaud, PhD Arnaud Mialon, PhD Saverio Priori, PhD
<b>Abstract:</b>	<p>This study is based on the analysis of detailed measurements of firn dielectric properties performed in Antarctica through coring down to 106 meters. Dielectric measurements in the frequency band (0.4 - 2.5 GHz) have been carried out using an open-resonator probe. Density was also measured for the same samples. The experimental results confirmed the well-known dependence of the real part of permittivity <math>\epsilon'</math> on depth and density, showing an increase of <math>\epsilon'</math> with density. The imaginary part also increases with depth with a rather complex dependence on frequency, probably due to the presence of salts or impurities. The analysis of the experimental data was performed by implementing 3D and 2D full wave numerical models, to simulate a mixture of firn crystals at prescribed densities, corresponding to the measured densities on the ice cores. The numerical analysis of the ensemble of inclusions showed that the usual symmetric formulae used for modeling ice dielectric properties agree with the average results of the simulation but they are not able to explain the spreading of the measured data at given density. A dielectric model was developed allowing for quantification of the dependence of dielectric properties on density, by combining two models: one consisting in firn crystals into an air host, the other assuming the presence of air inclusions into an homogeneous firn host. The weighted equation is based on the volume fraction. A simple geometric shape (ellipsoidal) is assumed for both ice crystals and air inclusions. This kind of shape is reasonable for the purpose of the dielectric study. The result is a mixture, smoothly changing from firn particles in air (low density) to air bubbles in an ice matrix (high density). A statistical analysis has been accomplished to investigate the dependence of the dielectric properties on the geometrical arrangement of the inclusions. For that purpose, a large number of simulations with different arrangements (micro-states) giving rise to the same average density (macro-state) has been carried out. The permittivity change due to micro-state variability appears to be at least two-three times the model variation due to density alone, and comparable to the measured variability at a given depth, suggesting that firn structure has a significant effect on the dielectric properties.</p>
<b>Suggested Reviewers:</b>	Udo Kaatze, PhD Professor, Georg-August-Universität Göttingen udo.kaatze@phys.uni-goettingen.de World leading expert in dielectric spectroscopy and EM methods  Frank Daschner, PhD Chair of Microwave Engineering, Christian-Albrechts-Universität zu Kiel

	<p>fd@tf.uni-kiel.de  Expert on microwave spectroscopy and engineering. Published many papers on cavity resonators (used in this study) on a variety of media.</p>
	<p>Yuri F Feldman, PhD  Professor, Hebrew University of Jerusalem  yurif@vms.huji.ac.il  World expert in the field of EM methods and dielectric spectroscopy. Authors of books and many papers. Performed research and published on the dielectric properties of snow and ice.</p>
	<p>Tuami Lasri, PhD  Professor, NRC National Institute for Nanotechnology  tuami.lasri@iemn.univ-lille1.fr  Expert in dielectric spectroscopy and micro electronics. He published many papers on dielectric spectroscopy and modelling.</p>
	<p>Shin SUGIYAMA, PhD  Professor, Hokkaido University  sugishin@lowtem.hokudai.ac.jp  Expert on Antarctic firn. He performed research on dielectric measurement on Antarctic Ice. Performed extended measuring campaigns.</p>

Investigating the influence of the grain size and  
distribution on the macroscopic dielectric  
properties of Antarctic Firn

R. Olmi<sup>1</sup>, M. Bittelli<sup>2</sup>, G. Picard<sup>3</sup>, L. Arnaud<sup>3</sup>, A. Mialon<sup>4</sup>, and S.  
Priori<sup>1</sup>

<sup>1</sup>Istituto di Fisica Applicata (IFAC), Consiglio Nazionale delle  
Ricerche (CNR), Sesto Fiorentino, Italia

<sup>2</sup>Dipartimento di Scienze e Tecnologie Agro-Alimentari (DISTAL),  
Università di Bologna, Italia

<sup>3</sup>UGA, CNRS, Institut des Géosciences et de l'Environnement  
(IGE), Grenoble, France

<sup>4</sup>CESBIO, Université de Toulouse,  
CNES/CNRS/INRAE/IRD/UPS, Toulouse, France

April 2020

# 1 Abstract

2 This study is based on the analysis of detailed measurements of firn dielectric  
3 properties performed in Antarctica through coring down to 106 meters. Dielec-  
4 tric measurements in the frequency band (0.4 – 2.5 GHz) have been carried out  
5 using an open–resonator probe. Density was also measured for the same sam-  
6 ples. The experimental results confirmed the well–known dependence of the  
7 real part of permittivity  $\epsilon'$  on depth and density, showing an increase of  $\epsilon'$  with  
8 density. The imaginary part also increases with depth with a rather complex  
9 dependence on frequency, probably due to the presence of salts or impurities.

10 The analysis of the experimental data was performed by implementing 3D  
11 and 2D full wave numerical models, to simulate a mixture of firn crystals at  
12 prescribed densities, corresponding to the measured densities on the ice cores.  
13 The numerical analysis of the ensemble of inclusions showed that the usual  
14 symmetric formulae used for modeling ice dielectric properties agree with the  
15 average results of the simulation but they are not able to explain the spreading  
16 of the measured data at given density.

17 A dielectric model was developed allowing for quantification of the de-  
18 pendence of dielectric properties on density, by combining two models: one  
19 consisting in firn crystals into an air host, the other assuming the presence of  
20 air inclusions into an homogeneous firn host. The weighted equation is based on  
21 the volume fraction. A simple geometric shape (ellipsoidal) is assumed for both  
22 ice crystals and air inclusions. This kind of shape is reasonable for the purpose  
23 of the dielectric study. The result is a mixture, smoothly changing from firn

24 particles in air (low density) to air bubbles in an ice matrix (high density).

25       A statistical analysis has been accomplished to investigate the dependence  
26 of the dielectric properties on the geometrical arrangement of the inclusions.  
27 For that purpose, a large number of simulations with different arrangements  
28 (micro–states) giving rise to the same average density (macro–state) has been  
29 carried out. The permittivity change due to micro–state variability appears  
30 to be at least two–three times the model variation due to density alone, and  
31 comparable to the measured variability at a given depth, suggesting that firn  
32 structure has a significant effect on the dielectric properties.

33       Keywords: Antarctica, dielectric measurements, ice cores, dielectric model,  
34 full wave EM simulations, close-off, firn

## 35 **2 Introduction**

36 Remote sensing techniques employed to measure Antarctica ice thickness, such  
37 as radars or radiometers, require an accurate estimation of ice dielectric prop-  
38 erties. The real and imaginary part of ice permittivity is one of the most im-  
39 portant variables determining the penetration depth or scattering of EM waves.

40       A variety of studies have been presented in the last decades to propose  
41 models of electric permittivity of snow and firn. An early work by Polder and  
42 van Santen (1946) computed the effective permittivity of a material consisting  
43 of a host medium in which solid particles or empty holes, assumed of ellip-  
44 soidal shape, are packed together. Tiuri et al. (1984) measured the complex

45 permittivity of firn at microwave frequencies, concluding that it is practically  
46 independent of the microstructure for density up to  $500 \text{ kg m}^{-3}$ . Matzer (1996)  
47 measured the permittivity of dry snow in 90 samples at different sites in the  
48 Swiss and Austrian Alps and showed the strong dependence of the real part of  
49 snow permittivity on density. The author also presented a formulation based on  
50 the effective medium formula (Polder and van Santen, 1946), and he concluded  
51 that the formulation for oblate spheroidal particles was the most appropriate  
52 and that the structure of the firn crystals have an effect on permittivity.

53       The transition between snow, firn and ice is based on density. Firn be-  
54 comes ice when the interconnecting air- or water-filled passageways between  
55 the grains are sealed off, a process called pore close-off. This value depends  
56 on density and it usually occurs around a density of  $830 \text{ kg m}^{-3}$  (Cuffey and  
57 Paterson, 2010). In this study we will refer to firn, since the measured densities  
58 are usually below this threshold.

59       A general overview of the different electromagnetic mixing models was  
60 presented by Sihvola (1999), discussing a variety of approaches including clas-  
61 sic mixing approaches, homogeneous and in-homogeneous inclusions, isotropic  
62 and anisotropic media and others. Among the various models, the continu-  
63 ous or bi-continuous random structure models showed promising results in the  
64 interpretation and modeling of dielectric spectroscopy or remote sensing data.  
65 Karkkainen et al. (2000) presented a numerical analysis of electromagnetic fields  
66 in random dielectric materials. The calculated permittivity distribution were  
67 compared with theoretical mixture models. They concluded that all the possible



68 permittivity values lie between the Wiener limits, and the values were almost  
69 always between the Hashin–Shtrikman limits.

70       When studying the dielectric properties of firn the most relevant variables  
71 are the density, at a macroscopic level, and orientation, size and shape of ice  
72 crystals on a microscopic scale. The crystal size can be represented by the  
73 average crystal area (Jun and Jacka, 1999), defined as the surface of an ellipse  
74 whose long and short semi-axes correspond to the radii of the largest inscribed  
75 circle and the smallest circumscribed circle, respectively, for a given crystal. The  
76 average crystal area of Antarctic firn is a function of depth. Crystal orientation,  
77 expressed for example by the crystallographic c-axis, has been shown to be  
78 practically random in polar ice cores (Jun and Jacka, 1999). If the crystal  
79 is roughly represented by an ellipsoid, which is acceptable for the purpose of  
80 the dielectric model, another parameter possibly influencing permittivity is the  
81 aspect ratio, which is descriptive of the crystal shape.

82       From the dielectric point of view, firn is modeled as a binary mixture,  
83 made of “pure” firn/ice and air. Different approaches (Sihvola, 1999) bring to  
84 symmetric formulae, where inclusions and host can be interchanged with no  
85 consequence on the effective permittivity, or to non–symmetric formulae based  
86 on the Maxwell Garnett theory, where the host material is that having the  
87 dominant volume fraction.

88       An analytic formula is only able to represent the average measured di-  
89 electric constant as a function of density or volume fraction. The choice of a  
90 non–symmetric model involving firn inclusions in air appears reasonable for

91 low-density material, while it does not appear meaningful for high-density  
92 material where a suspension of air bubbles into an ice host is physically more  
93 based. No analytic formula is able to handle inclusions having different shapes,  
94 size and orientation. Therefore a numerical method of analysis is needed.

95       Direct measurements of the dielectric properties of Antarctic ice, such as  
96 “dielectric profiling” (DEP) measurements on sampled firn cores, are scarcely  
97 common in the literature. The first comprehensive measurement was performed  
98 by Moore (1988), with a profiled firn core of 130 m depth in Antarctica, to mea-  
99 sure the reflection coefficient and electrical conductivity to derive the dielectric  
100 properties. However, the measurement was limited to the range of 20 Hz to  
101 300 kHz. Wolff et al. (1997) and Wolff (2000) focused on conductivity measure-  
102 ments, but the early attempts to measure firn’s permittivity by DEP (Moore,  
103 1988) were not pursued with more extensive campaigns and at higher frequen-  
104 cies of interest for space-borne radar and radiometers. Suguyama et al. (2010)  
105 measured the permittivity of the upper 1 meter snow layer at 35 locations, along  
106 a transect of approximately 50 km, using a transmission-line resonator. The  
107 measurements provided information in the horizontal direction, but to a shallow  
108 depth of 1 meter. Grimm et al. (2015) analyzed dielectric spectra (0.1 Hz – 1  
109 MHz) of 49 firn samples in Antarctica. However, they did not explore higher  
110 frequencies and did not collect detailed and extensive measurement on a single  
111 core down to over 100 meters depth. Overall, there is need to obtain detailed  
112 DEP in depth (at least at up to the close-off) in the frequency bands where  
113 space-borne radar and radiometers operate.

114 This study reports the results of direct measurement of dielectric prop-  
115 erties, density and specific surface area, performed at Dome-C in Antarctica  
116 (Concordia Experimental Station) down to 106 meters, through the collection of  
117 firn cores. The dielectric measurements were performed by an open-resonator  
118 probe (Olmí et al., 2019), providing high accuracy measurements of both the  
119 real and the imaginary parts, in four narrow frequency bands around 400, 880,  
120 1100 and 2500 MHz, as a function of depth  $z$  and density  $\rho$ . Measurements of  
121 the complex permittivity of firn were performed in situ and later repeated on the  
122 same samples transported in a cold laboratory. For the aim of interpreting the  
123 variability of experimental permittivity at given density, two- and three- di-  
124 mensional numerical models has been implemented, based on the Finite Element  
125 (FE) method. Computed dielectric permittivities are compared to experimental  
126 data and to existing mixture models to obtain a formulation for firn permittivity  
127 allowing to take in account the variability due to the microscopic arrangement  
128 of firn crystals.

### 129 **3 Materials and Methods**

130 The dielectric measurements described here have been conducted at the Concor-  
131 dia Station in Antarctica (73°30'S 123°00'E), on a core of firn drilled down to 106  
132 meters depth. Measurements were performed on core slices of 10 cm thickness,  
133 whose density was also measured and recorded. A total of 930 samples have  
134 been measured *in situ*, i.e. one every 10 cm, with two different open-coaxial

135 resonant probes, the first operating at about 900 MHz in air (2700 MHz in  
136 second harmonic), the second at 400 MHz in air (1200 in second harmonic).  
137 Measurements concerned depths from about 3 to 106 m, because the first 3 me-  
138 ters of core were damaged. Sample temperature was -20 °C. The samples were  
139 later moved into a cold laboratory in Firenze (Italy), where measurements were  
140 repeated at -19 °C, on 92 samples spaced about 1 m between them. In both  
141 cases only one point per sample was measured, with the exception of a limited  
142 number of them for testing purposes.

143       The electromagnetic technique used for dielectric measurement, based on  
144 a open-resonator probe, is thoroughly described in Olmi et al. (2019). The  
145 frequency band of interest for the study is 400–2500 MHz, because of the remote  
146 sensing applications relevant for the study itself.

147       The density of the samples used for dielectric measurements was directly  
148 deduced from mass and volume measurements. The diameter and height of each  
149 sample, assumed to be cylindrical in shape, were measured with a caliper, and  
150 mass was measured with a precision balance. Largest uncertainty came from the  
151 volume measurement, and accuracy of such density measurements on cohesive  
152 firn core samples is estimated to be better than 10 %.

153       In this work we will not be concerned with the variation of dielectric  
154 properties with frequency, the attention being focused on the dependence of  
155 permittivity on firn structure at a fixed frequency. Therefore, we will refer all  
156 future considerations to a nominal frequency of 1 GHz, although the data are  
157 shown for the measured frequencies.

## 158 **4 Theory**

### 159 **4.1 Numerical Simulation**

160 The dielectric model consists in a host medium containing a random distribution  
161 of inclusions (spheres, ellipsoids), of different size and orientation, possibly over-  
162 lapping. The host medium can be air and the inclusions ice crystals, or the op-  
163 posite. Borrowing the notion from statistical physics, we define “micro–state”  
164 a specific geometrical arrangement of inclusions. The average physical proper-  
165 ties (the “macro–state”) are obtained in principle by averaging on all possible  
166 micro–states. Therefore, generating geometrical arrangements corresponding  
167 to the same material density, we can compute the macro–state permittivity by  
168 averaging on the micro–states. At the same time, by looking at the statisti-  
169 cal distribution of the micro–state permittivity we obtain information on the  
170 influence of the geometrical arrangement on the complex permittivity variation.

171 Both three–dimensional (3D) and two–dimensional (2D) models have  
172 been implemented. The composite material fills a section of a parallel–plate  
173 wave–guide supporting a transverse electromagnetic (TEM) propagation mode.  
174 In the 3D case, the parallel–plate guide is realized by imposing a “perfect–magnetic  
175 wall” condition on two surfaces normal to the magnetic field vector, as shown  
176 in Figure 1. The EM wave, propagating along the  $y$  direction, has the electric  
177 field polarized in the  $z$ –direction and the magnetic field in the  $x$ –direction.  
178 The input port is the  $y=0$  plane, while a perfect electric reflector is placed at a  
179 distance  $d$  from it.

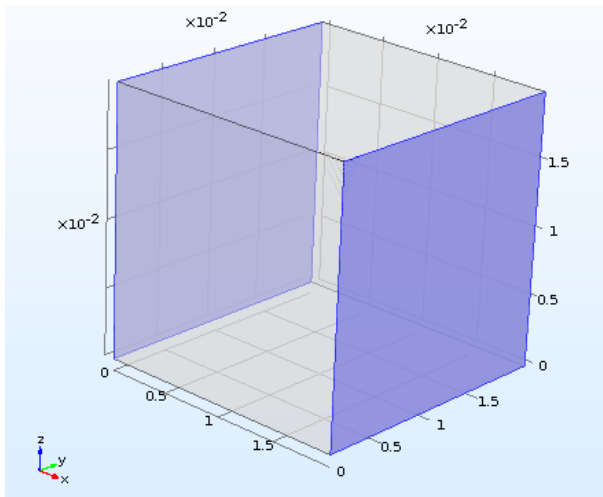


Figure 1: Geometry of the TEM waveguide. Electric field is  $z$ -directed, magnetic field is  $x$ -directed, wave propagation is along  $y$ . The “grayed” surfaces are the perfect magnetic walls.

180       Computing permittivity by means of the 3D model is very time-consuming,  
 181 in particular for densities that require a large partial volume fraction of the “in-  
 182 clusion” phase. The statistical analysis to be performed on the ensembles of  
 183 micro-states, requires the electromagnetic computation to be repeated hun-  
 184 dreds of times for a given density value. It was observed that, for a given  
 185 density, the distribution of the real and imaginary parts are practically identi-  
 186 cal for a 3D model of prolate spheroids and for a 2D model of ellipses, having  
 187 semi-axes and orientation in the same range of values. As an example, figure 2  
 188 respectively refer to 3D and 2D distributions giving rise to a firm density of 800  
 189  $\text{kg m}^{-3}$ .

190       The difference among 3D and 2D simulation is not only in the additional  
 191 dimension of the former, which dramatically increases the number of degrees

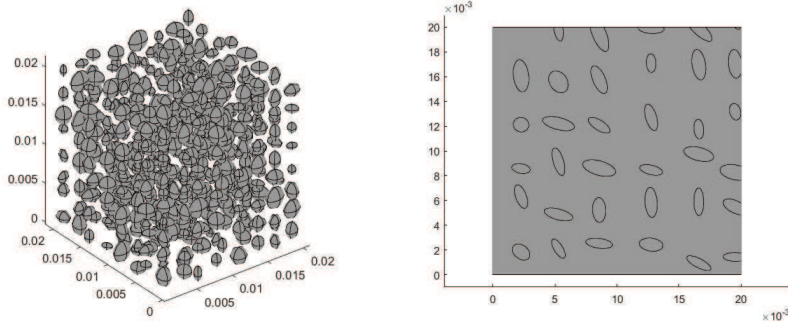


Figure 2: 3D distribution of spheroids and 2D distribution of ellipses (air inclusions in firn) corresponding to an firn density of  $800 \text{ kg m}^{-3}$ .

192 of freedom of the FEM problem (or, in other terms, the order of the system of  
 193 equations to be solved). Both in the 3D and 2D case, the inclusions are modeled  
 194 as geometric parts and, as such, they require to be meshed (with tetrahedra in  
 195 the 3D case or triangles in 2D). As a consequence, a geometry having a large  
 196 number of inclusions, possibly overlapping, requires a huge number of mesh  
 197 elements. Our approach, in the 2D case, is to generate the proper geometry  
 198 (i.e. the distribution of inclusion giving the required average density of firn) and  
 199 to include the information about the inclusion topology in a space-dependent  
 200 permittivity  $\epsilon(x, y)$ , which is a continuous analytical function. Although that  
 201 function has sharp edges at the interface between two materials (host/inclusion),  
 202 the geometry and the mesh topology of the problem remain unchanged.

203 Table 1 shows the differences between 2D and 3D for 400 micro-states,  
 204 for a material having a density  $\rho = 800 \pm 0.36\% \text{ kg m}^{-3}$ .

205 The almost perfect equivalence among 3D and 2D models suggests re-

Table 1: Comparison between the 3D and 2D mode

3D		2D	
$\epsilon'$	$\epsilon''$	$\epsilon'$	$\epsilon''$
$2.8 \pm 2.5\%$	$1.25 \times 10^{-3} \pm 4.7\%$	$2.8 \pm 2.3\%$	$1.32 \times 10^{-3} \pm 4.5\%$

206 sorting to a 2D model for the statistical purpose. The electromagnetic model  
 207 used to compute the complex permittivity of firm is reduced to a section of  
 208 parallel-plate waveguide, excited at one end (input port) by a TEM mode and  
 209 short-circuited at the other end (Figure 3).

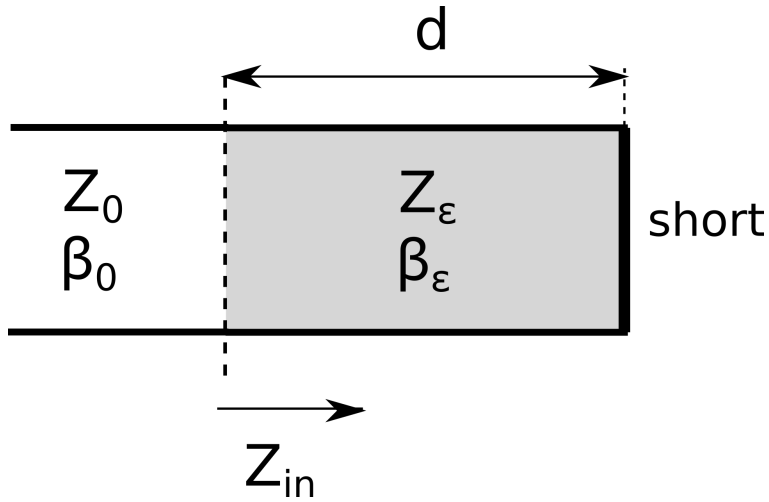


Figure 3: Transmission line equivalent circuit of the plane-wave propagation problem

210 The complex reflection coefficient computed at the input port contains the  
 211 information about the permittivity of the material filling the waveguide. The  
 212 choice of a full-wave solution, analogous to what proposed in Karkkainen et al.  
 213 (2000), has been preferred to the quasi-static approach proposed by Tuncer



214 et al. (2001) and frequently used in the modeling of random media, e.g. in Zhao  
 215 et al. (2004). The reason is that while the scale of the inclusions is such to fulfill  
 216 the requirements for a quasi–static approximation at about 1 GHz, the necessity  
 217 of having a sufficient volume (surface in 2D) to include a suitable number of firn  
 218 particles of different size brings to a macroscopic dielectric sample whose size is  
 219 not sufficiently smaller than the wavelength in firn. If the mean surface of the  
 220 inclusions is in the order of  $1 \text{ mm}^2$ , simulating firn with porosity 0.5, a sample  
 221 surface of  $1000 \text{ mm}^2$  contains 500 inclusions. Assuming a rectangular sample  
 222 surface, the characteristic length (CL) is in the order of the square root of 1000,  
 223 which is about  $1/10$  of the wavelength in air, and  $1/6$  of the wavelength ( $\lambda$ ) in  
 224 firn. These values are too large for a quasi–static approximation, requiring at  
 225 least  $\text{CL} < \lambda/20$ .

226 The reflection coefficient at the input of the firn–filled space is computed  
 227 in terms of the impedance  $Z_{in} = jZ_\epsilon \tan(\beta d)$  at the same interface:

$$\Gamma_{in} = \frac{Z_{in} - Z_0}{Z_{in} + Z_0} = \frac{j \tan(\beta d) - \sqrt{\epsilon}}{j \tan(\beta d) + \sqrt{\epsilon}} \quad (1)$$

228 where:

$$\beta = k_0 \sqrt{\epsilon} \quad (2)$$

$$Z_\epsilon = Z_0 / \sqrt{\epsilon} \quad (3)$$

229 are the complex wave number and characteristic impedance in firn, respectively,

230 while  $k_0$  and  $Z_0$  are the same quantities in air. The reason for including a “vir-  
 231 tual” section in air (actually, it is zero length) is that the FEM code normalizes  
 232 the computed scattering parameters to the free space impedance. The algo-  
 233 rithm for computing the complex permittivity  $\epsilon$  uses a FEM engine, based on  
 234 COMSOL Multiphysics<sup>®</sup>, integrated in MATLAB<sup>®</sup> code by LiveLink<sup>®</sup>.

235 The procedure for computing  $\epsilon$  is the following. Given the desired density  
 236 value  $\rho_D$ , distributions of ellipses with random orientation (between 0 and  $\pi/2$ )  
 237 are generated to fulfil a requirement about the “computed” density  $\rho_C = \rho_D \pm$   
 238  $\Delta$ . An algorithm was written in MATLAB<sup>®</sup> to generate a certain number of  
 239 particles of variable size and shape at spatial intervals (fixed on physical basis,  
 240 as described later), to achieve a target density corresponding to the measured  
 241 density as function of depth. During the iterations the algorithm adjusts the  
 242 lengths of the semi-axes, the aspect ratio (AR) and the angle of the generated  
 243 ellipses.

244 The complex permittivity  $\epsilon$  computed inverting (1) for density values  $\rho_C$   
 245 belonging to the interval  $(\rho_D - \Delta, \rho_D + \Delta)$  automatically takes into account the  
 246 dependence on density. The operation of inverting (1) maps the  $\Gamma$  interval onto  
 247 an  $\epsilon$  interval, depending on the density variation:

$$(\Gamma(\rho_D - \Delta), \Gamma(\rho_D + \Delta)) \rightarrow (\epsilon(\rho_D - \Delta), \epsilon(\rho_D + \Delta))$$

248 In relatively shallow firn the average crystal area (ACA) of Antarctic  
 249 firn/ice increases about linearly with depth. From Lipenkov et al. (1989) and  
 250 Jun and Jacka (1999) the ACA changes from about 0.4–0.9 mm<sup>2</sup> at a depth of

251 10 m to 1.4–1.6 mm<sup>2</sup> at 100 m. Arnaud et al. (1998) presented experimental  
252 data and a physical model (Arnaud et al., 2000) on the transformation of dry  
253 snow to firn and the of snow/firn and ice in the upper part of the polar sheets.  
254 Few data are available concerning the dependence of crystal orientation on depth  
255 for shallow firn, but it is reasonable (see, for example Jun and Jacka (1999))  
256 to assume a random orientation for the *c*-axis. Moreover, the orientation of  
257 elliptical inclusions does not have a marked effect on the average permittivity  
258 in a medium with randomly oriented inclusions (Sihvola, 1999), as an expected  
259 effect of the random dipole polarization moment. That characteristic has been  
260 confirmed by the numerical simulations described later in this paper.

261 In Azuma et al. (1999) the aspect ratio at the lowest reported depth (about  
262 100 m) is about 1.7. We can reasonably assume a linear dependence of the  
263 average aspect ratio between 1 and about 2 from the surface to 100 m depth,  
264 as an effect of firn compression.

265 For each density, a number (*e.g.* 100) of simulations are conducted to  
266 investigate the dependence of the dielectric properties on the micro-state con-  
267 figurations. From experiments, the dependence of density with depth is known.  
268 For each couple (depth, density) set in the numerical model, the average aspect  
269 ratio and the average particle diameter is fixed, and two sets of simulations are  
270 performed: one involving firn inclusions in air host medium, the other involving  
271 air inclusions in an ice host medium.

## 272 4.2 Dielectric mixing formulae

273 The effective permittivity of a random mixture (Sihvola, 2000) cannot be sum-  
274 marized by a closed-form analytic expression, although some work on the ana-  
275 lytical treatment of a dielectric containing random metallic inclusions has been  
276 done in the recent past (Koledintseva et al., 2006).

277 The results from numerical simulations of random inclusions in a host  
278 material do not agree with homogenisation formulas like that of Bruggeman  
279 (Sihvola, 1999) or, which is the same, the frequently used formula derived from  
280 the theory developed by Polder and van Santen (1946). The reason is that such  
281 formulae are symmetric in the permittivity of the inclusion material ( $\epsilon_i$ ) and of  
282 the host environment ( $\epsilon_e$ ):

$$(1 - v) \frac{\epsilon_e - \epsilon_m}{\epsilon_e + 2\epsilon_m} + v \frac{\epsilon_i - \epsilon_m}{\epsilon_i + 2\epsilon_m} = 0 \quad (4)$$

283 where  $\epsilon_m$  is the (effective medium) mixture permittivity and  $v$  is the volume  
284 fraction of the inclusion material. Numerically simulated dielectrics do not  
285 exhibit such a symmetry: the effective permittivity of an arrangement of ice  
286 inclusions in air, computed as a function of the density, is different from the  
287 permittivity of an arrangement of air inclusions in ice. As a consequence, if the  
288 inclusions were supposed to all have the same shape, the generalized Maxwell  
289 Garnett (MG) approach for ellipsoidal inclusions would be the correct choice  
290 (Sihvola, 1999). Actually, the MG formula is inherently non symmetrical so,  
291 given the density  $\rho$  of the material, and computing the air volume fraction  $v$  ( $\rho_I$

292 is the density of pure ice):

$$v = \frac{\rho_I - \rho}{\rho_I - 1} \quad (5)$$

293 leading to two different dielectrics: (1) an ice bulk medium containing a volume  
294 fraction  $v$  of air, or (2) an arrangement of firm inclusions having a total volume  
295 fraction  $1 - v$ , in air. Dielectrics (1) and (2) are described by two different MG  
296 formulas.

297 Just to show the connection between the MG approach and the Bruggeman  
298 formula, suppose the inclusions are oblate spheroids with semi-axis  $a$  and  $b$  in  
299 the ratio  $\theta = b/a = 2$ . The dielectric constant  $\epsilon_i$ , assumed real, of the inclusions  
300 can be that of ice (3.15) or air (1). Correspondingly, the dielectric constant of  
301 the external medium  $\epsilon_e$  will be 1 and 3.15, respectively.

302 Given the spheroid eccentricity  $e = \sqrt{\theta^2 - 1}$ , the MG formula for random  
303 inclusions involves the depolarization factors along axes parallel to the main  
304 directions (denoted by the numerals 1 to 3), given by (Sihvola, 1999):

$$A_1 = \frac{1 + e^2}{e^3} (e - \tan^{-1}(e)) \quad (6)$$

$$A_2 = \frac{1 - A_1}{2} \quad (7)$$

$$A_3 = A_2 \quad (8)$$

305 The effective MG dielectric constant  $\epsilon_M$  is:

$$\epsilon_M = \epsilon_e + \epsilon_e \frac{\frac{v}{3} \sum_{k=1}^3 f(\epsilon_i, \epsilon_e, A_k)}{1 - \frac{v}{3} \sum_{k=1}^3 A_k f(\epsilon_i, \epsilon_e, A_k)} \quad (9)$$

306 where:

$$f(\epsilon_i, \epsilon_e, A_k) = \frac{\epsilon_i - \epsilon_e}{\epsilon_e + A_k(\epsilon_i - \epsilon_e)} \quad (10)$$

307 By exchanging the role of inclusion and host, two non-intersecting curves  
 308 are obtained as function of the air volume fraction  $v$ . With reference to figure 4,  
 309 the dashed line is the dielectric constant of an ice host with air inclusions, while  
 310 the dotted curve is the dielectric constant of an air host with ice inclusions,  
 311 both as a function of the air volume fraction. The curves do not assume the  
 312 same value in  $v = 0.5$ , because of the formula asymmetry and, furthermore,  
 313 they have slightly different maximum and minimum values for pure ice (clearly  
 314 they coincide for  $v = 1$ , i.e. in pure air). But, if it is reasonable that quasi-pure  
 315 ice (e.g. at firn/ice transition where density is about  $830 \text{ kg m}^{-3}$ ) is “solid ice  
 316 with air bubbles”, and it is equally meaningful to consider snow as “ice crystals  
 317 suspended in air”, a transition between the upper and the lower model of Figure  
 318 4 must be defined.

319 The simplest transition is a linear transformation from the former (a/i: air  
 320 in ice) to the latter (i/a: ice in air), or in other words to compute the mixture  
 321 dielectric constant  $\epsilon_m$  as follows, where the inclusion volume fraction has been  
 322 substituted by the material density  $\rho$  which is the parameter of interest:

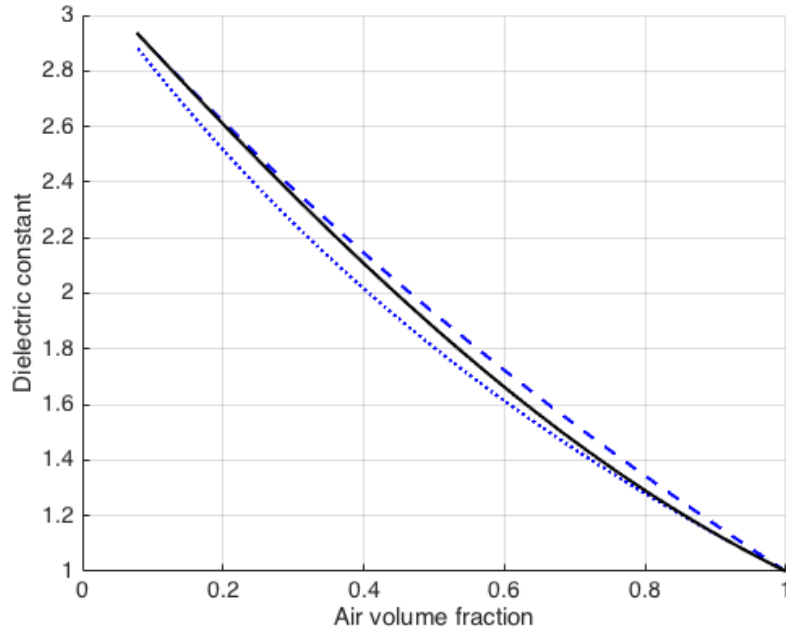


Figure 4: Dielectric constant of an ice/air mixture computed by the MG formula, as a function of the volume fraction (see text)

$$\epsilon_m(\rho) = [1 - \eta(\rho)] \epsilon_{i/a}(\rho) + \eta(\rho) \epsilon_{a/i}(\rho) \quad (11)$$

323 with:

$$\eta(\rho) = \frac{\rho - 1}{\rho_I - 1} \quad (12)$$

324 Such a linear relation is such that the dielectric constant for  $v = 0.5$  is  
 325 exactly the mean value between those of the upper and lower curves at the same  
 326 volume fraction. The solid line in figure 4, representing the linear transformation

327 from the a/i to the i/a model, almost perfectly corresponds with the dielectric  
328 constant computed by the Bruggeman formula (4), confirming the validity of  
329 the linear transformation. Figure 5 shows such a correspondence: the maximum  
330 percentage deviation from the Bruggeman formula is less than 0.7 %.

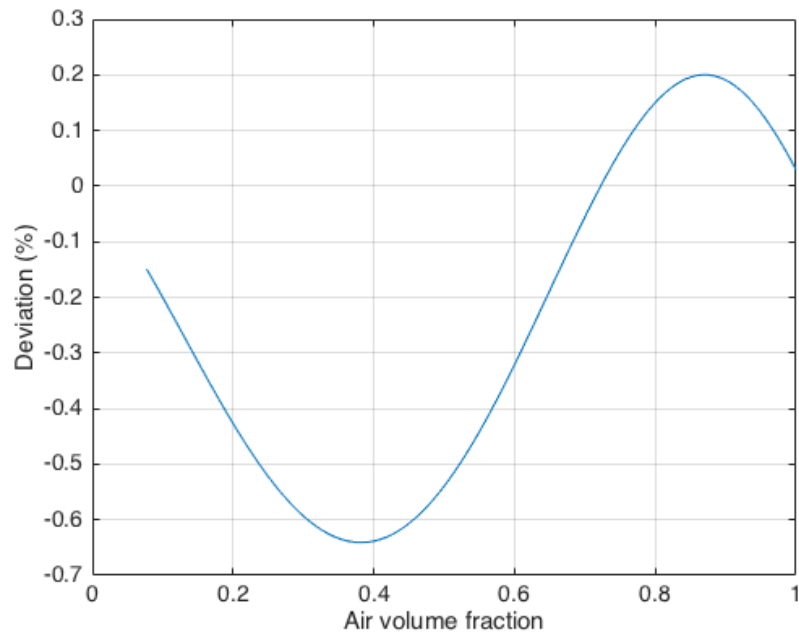


Figure 5: Relative percentage deviation of the linear formula (11) from the Bruggeman effective dielectric constant



## 331 5 Results

### 332 5.1 Experimental Results

333 The measurement procedure and, in particular, the electromagnetic model of  
334 the open-resonator probe, is described elsewhere (Olmí et al., 2019). Two  
335 cavity resonators are used, operating in first and second harmonics.

336 Briefly summarizing, for each cavity two calibration measurements are  
337 conducted – one in air, one with the probe placed on a reference dielectric –  
338 at the beginning and at the end of a session (usually half a day), after a full  
339 calibration of the vector network analyzer used to measure the transmission  
340 through the microwave cavity.

341 Figure 6 depicts the dielectric constant as function of depth at four fre-  
342 quencies (first and second resonant mode of the two cavity resonators employed),  
343 while figure 7 shows the measured loss tangent at the same frequency values.  
344 The smooth lines of both dielectric constant and loss tangent are a result of a  
345 “smoothed” calibration procedure, not of a direct smoothing or interpolation  
346 of the measured data. The transmission coefficient in every session is inverted  
347 to give the complex permittivity using the “local” calibration, i.e. that relative  
348 to the session (red dots). As an alternative, the calibration parameters at each  
349 frequency can be used to build a smoothed calibration curve, which brings to  
350 the solid-line values in figures 6 and 7.

351 It clearly appears that the real part of permittivity weakly depends on  
352 frequency and exhibit the same dependence with depth. The same is not true

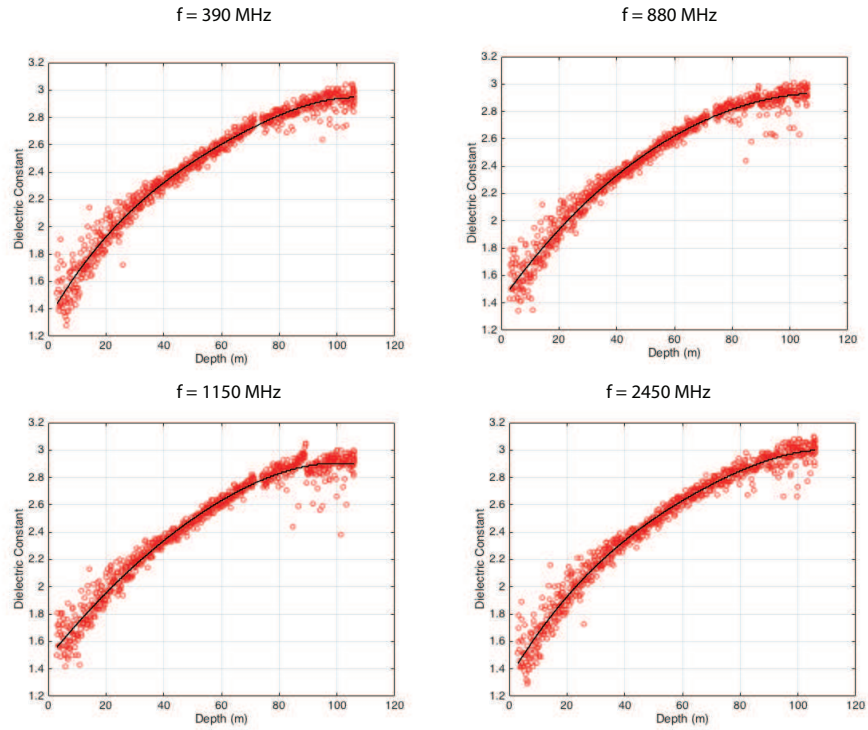


Figure 6: Real part of complex permittivity versus depth

353 for the imaginary part, whose dependence on frequency appears rather complex,  
 354 probably due to the presence of salts or impurities, although generally increas-  
 355 ing with depth. This could hopefully be confirmed by a cross-check with the  
 356 findings of physical-chemical analyses currently in progress.

357 Figure 8 shows the measured density of the core slices as a function of the  
 358 slice depth. The dependence of density  $\rho$  on depth  $z$  appears to be described  
 359 by a power-law relation:

$$\rho(z) = az^b + c \quad (13)$$

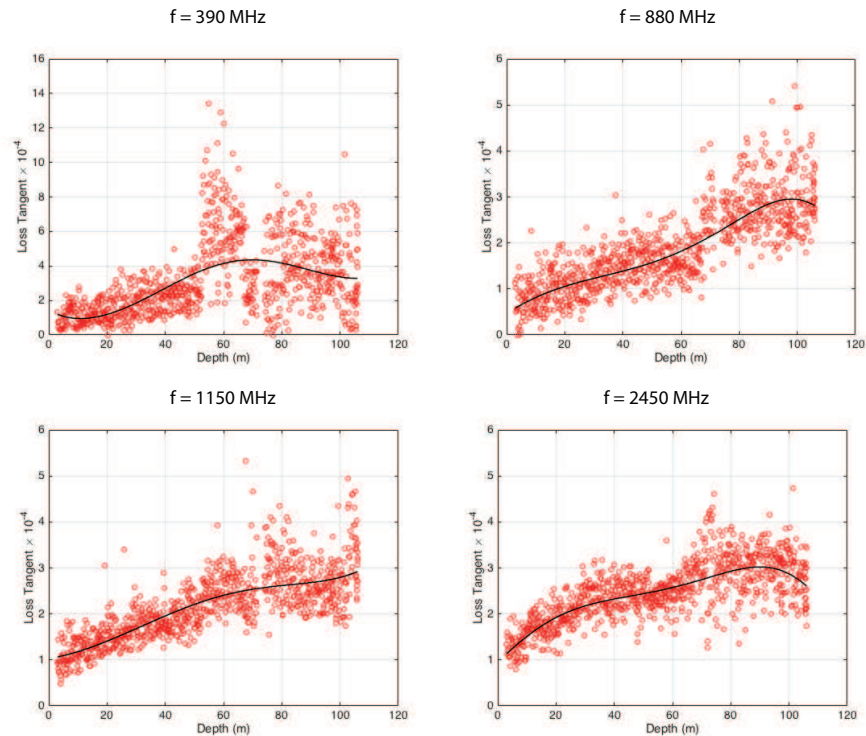


Figure 7: Loss tangent versus depth

360 which corresponds to the solid line in the figure. The dashed line refers to  
 361 the bi-exponential fitting model introduced by Arthern et al. (2013), whose  
 362 rationale is based on the existence of a critical density where a discontinuity  
 363 appears in the derivative of  $\rho(z)$ . That kind of relationship does not appear to  
 364 describe well our experimental data.

## 365 5.2 Numerical Results

366 Two sets of simulations are conducted, to follow the procedure summarized by  
 367 equation (11). The first set allows to compute  $\epsilon_{i/a}(\rho, z)$ , the second  $\epsilon_{a/i}(\rho, z)$ ,

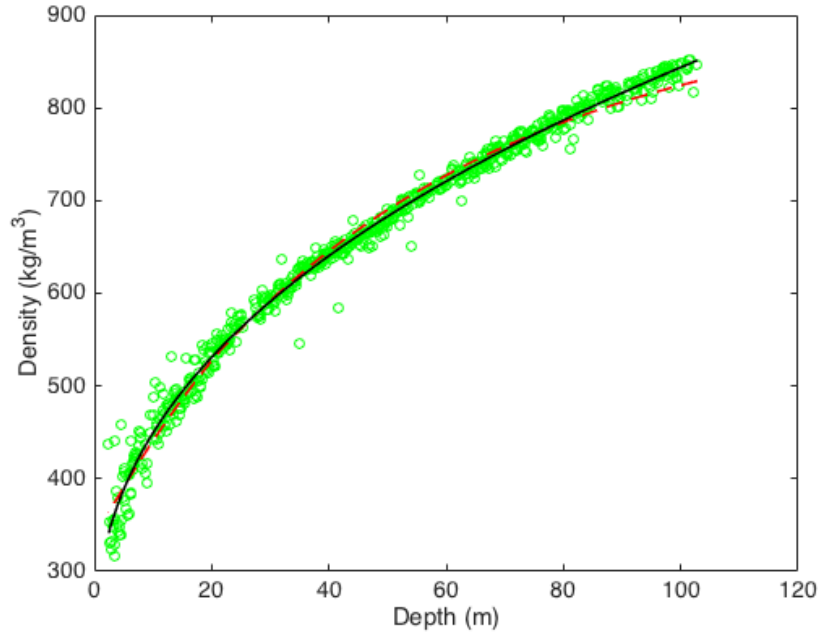


Figure 8: Density  $\rho(z)$  versus depth: comparison between the power-law fitting (solid black line) and the bi-exponential fitting (dashed red line)

368 where “i/a” and “a/i” mean “ice in air” and “air in ice” respectively, as in  
 369 Section 4.2.

### 370 5.2.1 Statistical Analysis

371 For each density value (macro-state) we obtain a set of micro-states by the  
 372 procedure outlined in the previous section. As an example, figure 9 (left) shows  
 373 a configuration of firn inclusions (black) in air (white) corresponding to a density  
 374 of  $400 \text{ kg m}^{-3}$ , and (right) a configuration of air inclusions (white) in a ice host  
 375 material (black). It is clear from figure 9 how the depth, hence the density,

376 plays a role in the variation of shape and size of the inclusions.

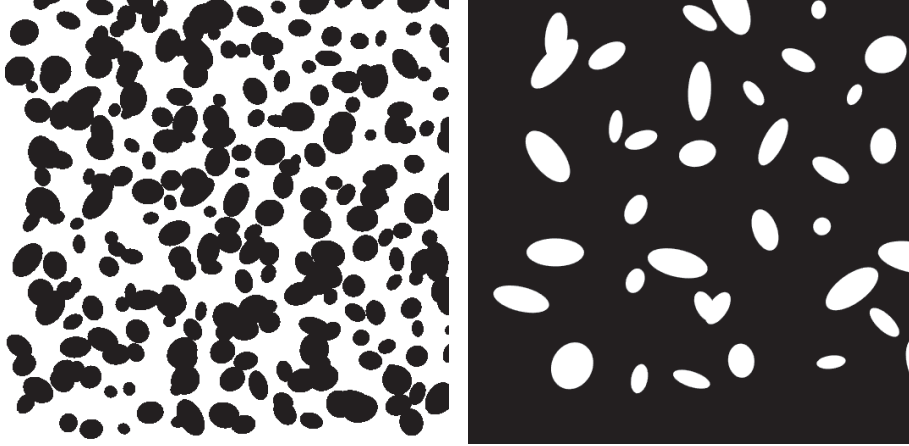


Figure 9: Micro-states.  $\rho = 400 \text{ kg m}^{-3}$  (left) and  $\rho = 800 \text{ kg m}^{-3}$  (right)

377 The density corresponding to a macro-state in a simulation is allowed  
378 to have a small interval of variation around the set value, to be able to apply  
379 a sort of de-trending to the computed complex permittivity values. In fact,  
380 although several formulas exist, see for example Kovacs et al. (1995), relating  
381 the real part of permittivity to density and, of course, a fitting of  $\epsilon$  versus  $\rho$  can  
382 be performed over the entire density range, we found that greater accuracy in  
383 de-trending is achieved by “zooming” into a small region of densities.

384 Denoting by  $\Delta\epsilon'$  and  $\Delta\epsilon''$  the de-trended values of  $\epsilon'$  and  $\epsilon''$ , we obtain  
385 from simulations the results presented in Figure 10 for a density of  $400 \text{ kg m}^{-3}$ .

386 Very similar results are obtained for a density of  $840 \text{ kg m}^{-3}$ , as depicted  
387 in Figure 11. To summarize, we observe that the dielectric constant (real part)  
388 has a  $3\sigma$  variation of 0.08 for each value in the whole density range. The  $3\sigma$

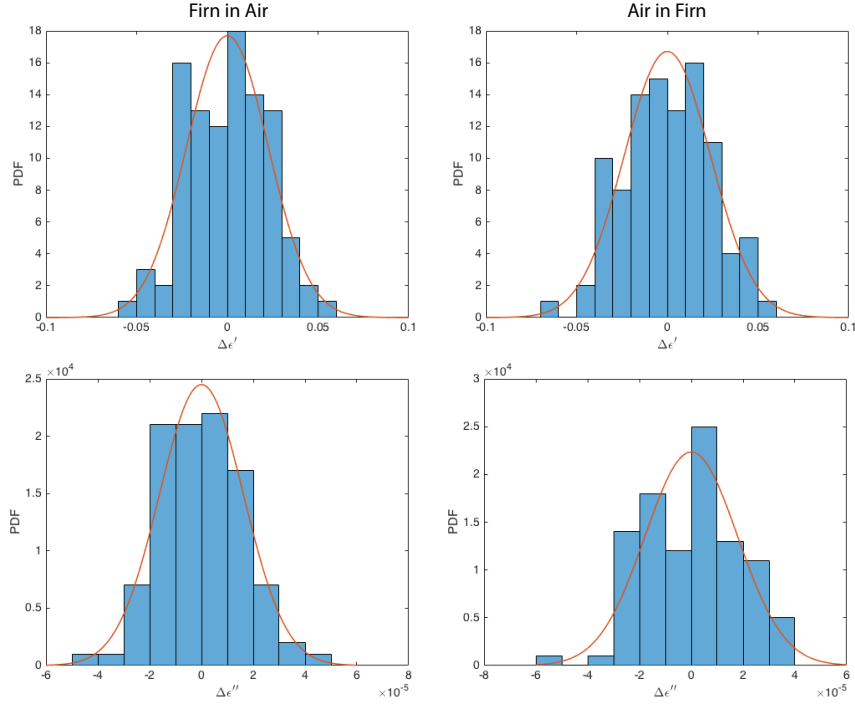


Figure 10:  $\Delta\epsilon'$  (top plates) and  $\Delta\epsilon''$  (bottom plates) for  $\rho = 400 \text{ kg m}^{-3}$

389 variation is  $6 \times 10^{-5}$  and  $9 \times 10^{-5}$  for dielectric losses at  $400 \text{ kg m}^{-3}$  and  $840 \text{ kg}$   
 390  $\text{m}^{-3}$  respectively. The micro-state variability is entirely responsible of such a  
 391 variation, as the change with density has been dropped out by the de-trending  
 392 procedure.

### 393 5.2.2 Discussion

394 Figure 12 compares the experimental results of  $\epsilon$  as a function of depth with  
 395 the results of the numerical model. The dashed lines are the  $\pm 3\sigma$  values around  
 396 the mean, i.e. the values between the dashed curves include about 99% of  
 397 the possible dielectric constants computed by the models as a function of the

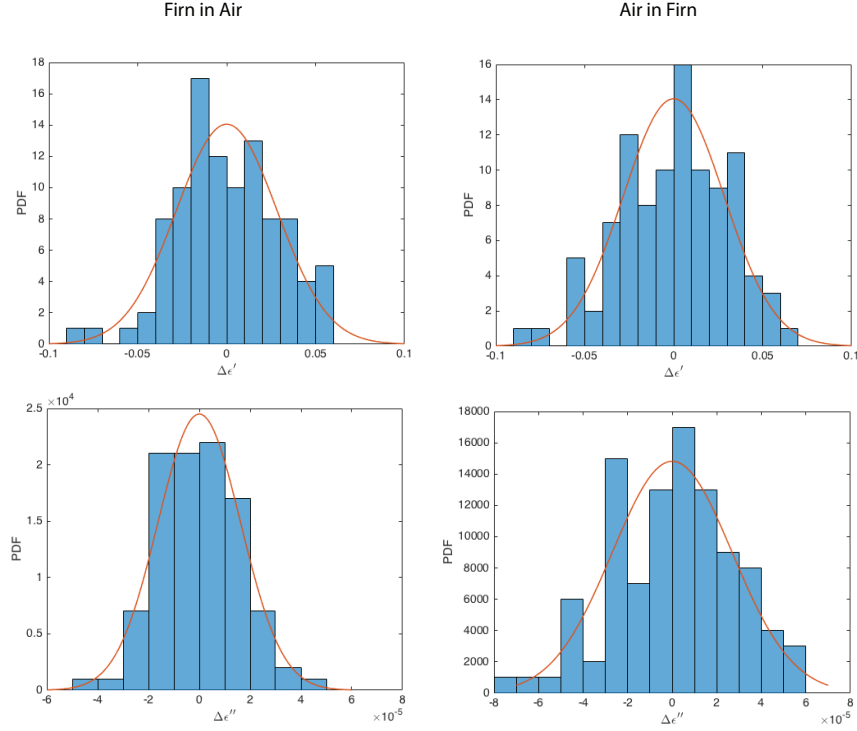


Figure 11:  $\Delta\epsilon'$  (top plates) and  $\Delta\epsilon''$  (bottom plates) for  $\rho = 840 \text{ kg m}^{-3}$

398 micro-state configurations. The solid line is computed applying the linear  
 399 relation (11), while the dash-dot line is computed by the Bruggeman formula.

400 The results on the statistical variation of the imaginary part, and hence  
 401 of the loss tangent, are similar. Of course, the computation of the imaginary  
 402 part of the ice/air mixture depends on the true value of the imaginary part of  
 403 pure ice at the frequency of interest, which is not so well defined as the real part  
 404 (Figure 13). As for the real part, the dashed lines correspond to  $3\sigma$  variation  
 405 around the mean value.

406 The average dielectric constant computed by (11), with the variance based

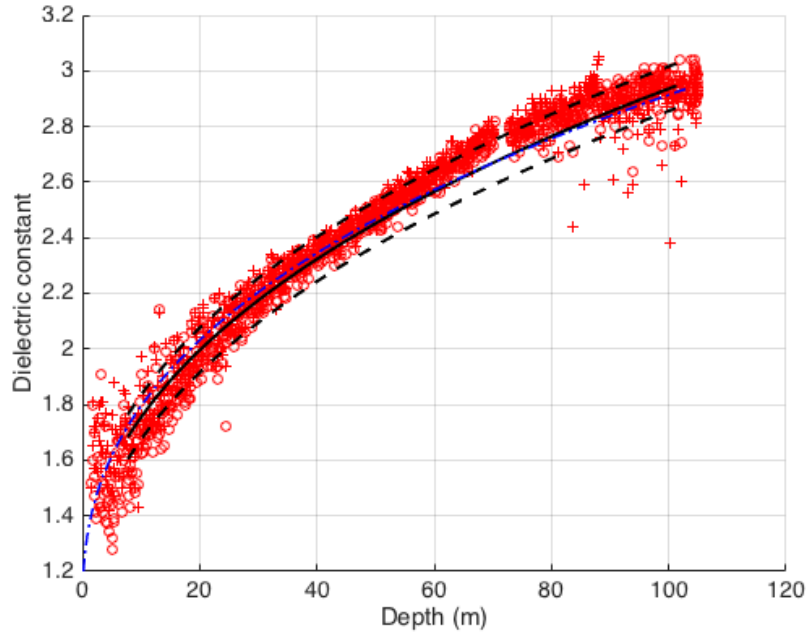


Figure 12: Dielectric constant versus depth: comparison between the experimental data at 880 MHz (red circles) and at 1.15GHz (red crosses) and the results of the full-wave numerical model at 1 GHz

407 on the statistical analysis, represents quite well the experimental behaviour, like  
 408 the Bruggeman formula does, only slightly over-estimating the dielectric con-  
 409 stant at low depth (lower than 20 meters), i.e. in the lower range of densities.  
 410 The statistical analysis allows to visualize the expected variability of the average  
 411 dielectric constant due to the micro-state variability. The variance of the ex-  
 412 perimental data at a given depth is very similar, although some outliers appear  
 413 as a consequence of the local variation of density at the close-off depths.



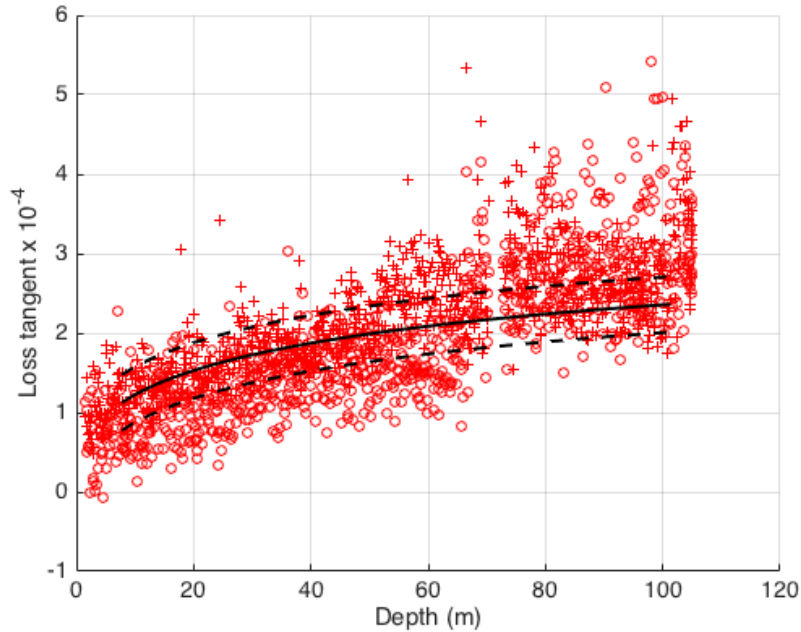


Figure 13: Loss tangent versus depth: comparison between the experimental data at 880 MHz (red circles) and at 1.15GHz (red crosses) and the results of the full-wave numerical model at 1 GHz

## 414 6 Conclusions

415 In this study detailed measurements of firm dielectric properties were performed  
 416 through the collection of firm cores down to 106 meters, by using a resonator.  
 417 Detailed measurements of the real and imaginary dielectric permittivity were  
 418 performed on the ice cores providing an extended dataset of dielectric properties  
 419 with depth. Density was also measured for the same samples. The experimental  
 420 results confirmed the dependence of the real part with depth and density. In-  
 421 creasing depth and density corresponds to an increase in the real permittivity.

422 A power–law equation was derived to fit the data. The imaginary part also  
423 increases with depth but it does not follow the same clear trend, its dependence  
424 on frequency appears rather complex, probably due to the presence of salts or  
425 impurities.

426 The analysis of the experimental data was performed by first implement-  
427 ing 3D and 2D full wave numerical models, by generating random ensembles of  
428 inclusions , to simulate a mixture of firn crystals at prescribed densities, corre-  
429 sponding to the measured densities on the ice cores. The numerical analysis of  
430 the ensemble of inclusions showed that the common symmetric functions used for  
431 ice dielectric properties do not agree with the results of the simulation and with  
432 the measured data. These results show that a host of ice crystals into air signif-  
433 icantly differs from a host of air bubbles into ice, and therefore non–symmetric  
434 formulations should be used. A single non–symmetric formulation is not suf-  
435 ficient to continuously represent the whole density range. Moreover, analytical  
436 formulae are unable to account for the effect of randomness, size/shape hetero-  
437 geneity, particle packing on the average firn permittivity.

438 To solve this problems a dielectric model was developed, allowing for quan-  
439 tification of the dependence of the dielectric properties on density. The model  
440 was developed by combining two models: one of firn crystals into an air host,  
441 and air inclusions into an ice host. The weighted equation is based on the vol-  
442 ume fraction (density). The result is a mixture smoothly changing from firn  
443 particles in air (low density) to air bubbles in an ice matrix (high density).  
444 The implementation of such a mixture model by means of a numerical model

445 allowed to investigate the dependence of complex permittivity at all densities  
446 in the range 350–840 kg m<sup>-3</sup>, on the average firn characteristics, e.g. crystal  
447 area, shape and orientation, and on the average crystal arrangement. For this  
448 purpose, a statistical analysis has been conducted showing how the variability  
449 of the micro–states affects the average permittivity. The permittivity change  
450 due to micro–state variability appears to be at least two–three times that due  
451 to the measured variability of density at a given depth, therefore concluding  
452 that firn structure has a significant effect on the dielectric properties.

## 453 **7 Acknowledgement**

454 This study was funded by PNRA (Progetti Nazionali di Ricerca in Antartide,  
455 Ministry of Education and Research, Rome, Italy) Research Project: Dielec-  
456 tric Characterization of the Polar Cap by perforations at Dome–C (PNRA16-  
457 00212), and by the Institut Paul Emile Victor (France). The ice core was ob-  
458 tained from the Centre de Carottage et de Forage National (France).

## 459 **References**

- 460 Arnaud, L., Barnola, J., Duval, P., 2000. Physical modelling of the densification  
461 of snow/firn and ice in the upper part of polar ice sheets, In: Physics of Ice  
462 Core Records, Hokkaido Univ. Press, Sapporo, Japan., pp. 285–305.
- 463 Arnaud, L., Lipenkov, V., Barnola, M., Gay, M., Duval, P., 1998. Modelling

464 of the densification of polar firn: characterization of the snow-firn transition.  
465 *Annals of Glaciology* 26, 39–44.

466 Arthern, R.J., Corr, H.F.J., Gillet-Chaulet, F., Hawley, R.L., Morris, E.M.,  
467 2013. Inversion for the density-depth profile of polar firn using a stepped-  
468 frequency radar. *Journal of Geophysical Research: Earth Surface* 118, 1257–  
469 1263.

470 Azuma, N., Wang, Y., Mori, K., Narita, H., Hondoh, T., Shoji, H., Watanabe,  
471 O., 1999. Texture and fabrics in the dome f (antarctica) ice core. *Annals of*  
472 *Glaciology* 29, 163–168.

473 Cuffey, K., Paterson, W., 2010. *The physics of glaciers*. volume ISBN 978-0-12-  
474 369461-4. fourth ed., Elsevier, Amsterdam.

475 Grimm, E., D.E.Stillman, MacGregor, J., 2015. Dielectricsignaturesand evolutio  
476 n of glacier ice. *J. Glaciol.* 61, 1159–1170.

477 Jun, L., Jacka, T.H., 1999. Crystal-growth rates in firn and shallow ice at  
478 high-accumulation sites. *Annals of Glaciology* 29, 169–175.

479 Karkkainen, K.K., Sihvola, A.H., Nikoskinen, K.I., 2000. Effective permittiv-  
480 ity of mixtures: Numerical validation by the fdtd method. *IEEE Trans. on*  
481 *Geosci. and Remote Sens.* 38, 1303–1308.

482 Koledintseva, M.Y., Chandra, S.K.R., DuBroff, R.E., Schwartz, R.W., 2006.  
483 Modeling of dielectric mixtures containing conducting inclusions with statis-

484 tically distributed aspect ratio. *Progress In Electromagnetics Research* 66,  
485 213–228.

486 Kovacs, A., Gow, A.J., Morey, R.M., 1995. The in-situ dielectric constant of  
487 polar firn revisited. *Cold Regione Science and Technology* 23, 245–256.

488 Lipenkov, V.Y., Barkov, N.I., Duval, P., Pimienta, P., 1989. Crystalline texture  
489 of the 2083 m ice core at vostok station, antarctica. *Journal of Glaciology* 35,  
490 392–398.

491 Matzer, C., 1996. Microwave permittivity of dry snow. *IEEE Trans. Geo.*  
492 *Remote Sens.* 34, 573–581.

493 Moore, J., 1988. Dielectric variability of a 130 m antarctice ice core: Implications  
494 for radar sounding. *Annals of Glaciology* 11, 95–99.

495 Olmi, R., Toccafondi, A., Priori, S., Puggelli, F., 2019. An open-resonator sensor  
496 for measuring the dielectric properties of antarctic ice. *Sensors* 19, 2099.

497 Polder, D., van Santen, J.H., 1946. The effective permeability of mixtures of  
498 solids. *Physica* 12, 257–271.

499 Sihvola, A., 1999. *Electromagnetic Mixing Formulas and Applications*. Electro-  
500 magn. waves ser. 47, ed., Inst. Electr. Eng., London.

501 Sihvola, A.H., 2000. Mixing rules with complex dielectric coefficients. *Subsurface*  
502 *Sensing Technologies and Applications* 1, 393–415.

503 Suguyama, S., Enomoto, H., Fujita, S., Fukui, K., Nakazawa, F., Holmlund, P.,  
504 2010. Dielectric permittivity of snow measured along the route traversed in

505 the japanese-swedish antarctic expedition 2007/08. *Annals of Glaciology* 51,  
506 9–15.

507 Tiuri, M., Sihvola, A., Nyfors, E., Hallikaiken, M., 1984. The complex dielec-  
508 tric constant of snow at microwave frequencies. *IEEE Journal of Oceanic*  
509 *Engineering* OE-9.

510 Tuncer, E., Gubanski, S.M., Nettelblad, B., 2001. Dielectric relaxation in dielec-  
511 tric mixtures: Application of the finite element method and its comparison  
512 with dielectric mixture formulas. *Journal of Applied Physics* 89, 8092–8100.

513 Wolff, E., 2000. Electrical stratigraphy of polar ice cores: Principles, methods,  
514 and findings, in: Hondoh, T. (Ed.), *Physics of Ice Core Records*. Hokkaido  
515 Univ. Press, Sapporo, Japan, p. 155–171.

516 Wolff, E., Miners, W., Moore, J.C., Paren, J.G., 1997. Factors controlling the  
517 electrical conductivity of ice from polar regions—a summary,. *J. Phys. Chem.*  
518 *B* 101, 6090– 6094.

519 Zhao, X., Wu, Y., Fan, Z., Li, F., 2004. Three-dimensional simulations of the  
520 complex dielectric properties of random composites by finite element method.  
521 *Journal of Applied Physics* 95, 8110–8117.

**Declaration of interests**

The authors declare that they have no known competing financial interests or personal relationships that could have appeared to influence the work reported in this paper.

The authors declare the following financial interests/personal relationships which may be considered as potential competing interests: